NOVEMBER 26 2018

Acoustically relevant properties of four crude oils at oceanographic temperatures and pressures

Scott Loranger; Christopher Bassett; Justin P. Cole; Bret Boyle; Thomas C. Weber

J. Acoust. Soc. Am. 144, 2926–2936 (2018)
https://doi.org/10.1121/1.5078606

Acoustically relevant properties of four crude oils at oceanographic temperatures and pressures

Scott Loranger,[1,a)] Christopher Bassett,[2] Justin P. Cole,[3] Bret Boyle,[3] and Thomas C. Weber[4]

[1]*Department of Earth Sciences, University of New Hampshire, Durham, New Hampshire 03824, USA*
[2]*National Marine Fisheries Service, Alaska Fisheries Service Center, Resource Assessment and Conservation Engineering Division, Seattle, Washington 98115, USA*
[3]*Department of Chemistry, Colorado State University, Fort Collins, Colorado 80526, USA*
[4]*Department of Mechanical Engineering, University of New Hampshire, 105 Main Street, Durham, New Hampshire 03824, USA*

(Received 10 July 2018; revised 24 October 2018; accepted 25 October 2018; published online 26 November 2018)

Inversions of models of broadband acoustic scattering to detect and quantify weakly scattering targets, such as oil droplets in seawater, require precise knowledge of the physical properties that determine scattering. When the characteristic impedance contrast between a target and the surrounding medium is weak, small differences between the true and modeled impedance can cause significant errors in modeled scattering. For crude oil, currently available empirical models of density and sound speed are derived from measurements made at reservoir conditions (high temperature and pressure), which may not be relevant to oceanographic conditions due to phase changes in the oil. Measurements of the density and sound speed, as well as thermal characterization of phase changes via differential scanning calorimetry, of four crude oils at oceanographically relevant temperatures and pressures were made and compared to a commonly used empirical model for sound speed and density. Significant deviations between the measured and modeled values were found and different empirically fit models were developed. A literature review of sound speed data was also performed, and the innovative empirical model shows improvement over the commonly used empirical model for both the data measured here and the measurements in the literature.

https://doi.org/10.1121/1.5078606

[JAC] Pages: 2926–2936

I. INTRODUCTION

At the end of the first quarter of 2018, almost 800 offshore drilling rigs were available for hydrocarbon extraction (IHS Markit, 2015). Over the past decade offshore oil production has accounted for approximately 30% of total oil production (U.S. Energy Information Administration, 2016). Advances in exploration and extraction technology have resulted in expansion of offshore production into new environments. While a majority of this oil is extracted from waters less than 125 m deep, increasingly large portions are extracted from depths in excess of 1500 m. This production occurs globally with rigs located in areas that cover the full range of oceanographic environments from warm tropical waters to seasonally ice-covered waters in the Arctic.

Many questions exist about the expected environmental impact of spills in the climatically and ecologically diverse environments where drilling occurs. Understanding potential environmental impacts due to spills and developing an appropriate response requires both the ability to quantify the total volume of oil spilled and knowledge of baseline levels of natural oil seepage. For example, the Deepwater Horizon spill released approximately 680 000 tonnes of oil (U.S. Library of Congress, 2011). The most recently available estimate of annual flux of liquid hydrocarbons from natural seepage in the Gulf of Mexico is between 80 000 and 200 000 tonnes of oil and between 200 000 and 2 000 000 tonnes worldwide (Transportation Research Board and National Research Council, 2003). Liquid hydrocarbon flux from the Deepwater Horizon spill is estimated to have been between 34% and 340% of the global annual flux of oil into the ocean. While any increase above background levels is likely to have an environmental impact, knowledge of the magnitude of a spill relative to background levels is necessary both to inform decision-making during spill response and assess the long-term impact on the environment. Acoustic methods (e.g., Camilli *et al.*, 2012; Weber *et al.*, 2012), offer a path toward quantifying both anthropogenically released and naturally occurring liquid hydrocarbons in the ocean, but are limited by the paucity of information describing the physical properties of oil needed for acoustic scattering models at oceanographic conditions. The present work seeks to address this information gap by reporting measurements of oil density and sound speed under pressure and temperature conditions relevant to much of the world's oceans, and by developing an empirical model for these properties that performs better than existing models for the types of oils studied.

[a)]Electronic mail: sloranger@ccom.unh.edu

Natural hydrocarbon seepage from the seafloor can take the form of free gas, hydrate-coated gas bubbles, and liquid oil, and occur throughout the world's oceans (Judd, 2003; Kvenvolden and Cooper, 2003; Sahling *et al.*, 2016). Seepage associated with free gas (with or without hydrate) is often detected and quantified acoustically, taking advantage of the large impedance contrast between free gas and seawater (Greinert *et al.*, 2006; Heeschen *et al.*, 2003; Merewether *et al.*, 1985; Römer *et al.*, 2012; Schneider von Deimling *et al.*, 2011; Weber *et al.*, 2014). The present study is aimed at the study and assessment of the seepage of liquid oil, such as the seeps reported in the Gulf of Mexico and the Congo Basin (Crooke *et al.*, 2015; Jatiault *et al.*, 2018; Roberts and Carney, 1997; Sahling *et al.*, 2016; Transportation Research Board and National Research Council, 2003). In deep water environments a variety of instrumentation is used for the detection and quantification of oil; however, most of these instruments are limited to short detection ranges on the order of meters, or even centimeters (e.g., fluorometers, mass spectrometers). Given this short detection range it is difficult to accurately evaluate the flux for an entire ocean basin or even a large spill. Acoustic instrumentation provides the potential for the detection and quantification of hydrocarbons at greater ranges. Active acoustic methods have been used to estimate the flux of oil from deep water blowouts (Camilli *et al.*, 2012), detect and quantify oil at ranges of up to hundreds of meters from the instrument (Weber *et al.*, 2012), and estimate the thickness of oil layers under sea ice (Bassett *et al.*, 2016; Pegau, 2017; Wilkinson *et al.*, 2015).

Quantifying oil acoustically, whether present as droplets or in layers, depends on a thorough understanding of the physical properties that determine acoustic scattering. The intensity of acoustic scattering is dependent on the geometry (e.g., the thickness of an oil layer or shape of a droplet) and the mismatch between the characteristic impedance (the product of density and sound speed) of the surrounding water and the target. In previous studies of crude oil, researchers have had to make assumptions about the physical properties of oil in order to estimate flux (Weber *et al.*, 2012).

One of the reasons that the acoustically relevant properties of crude oil (shape, size, density, and sound speed) are difficult to quantify is that the term "crude oil" encompasses a wide variety of unrefined liquid petroleum products that are composed of multiple hydrocarbon chains of different molecular weights in addition to other organic materials. Crude oils are often classified by their American Petroleum Institute gravity, API_g. This dimensionless quantity is related to the specific gravity of the liquid according to $API_g = 141.5/SG - 131.5$, where SG is the specific gravity of the liquid at 15.56 °C and 0.1 MPa. By this definition light crudes have an API_g higher than 31.1°, medium crudes have an API_g between 22.3° and 31.1°, and heavy to extra heavy crude oils have an API_g less than 22.3°. The concentration of hydrocarbon chains of differing length and geometry as well as organic material present generally varies based on the origin of the petroleum, and oils with similar API_g do not necessarily have the same distribution of hydrocarbon chains and organic materials.

The saturated hydrocarbon chains (also referred to as paraffins, waxes, or *n*-alkanes), which generally make up a significant percentage of the mass of crude oil, are prone to crystallization at temperatures and pressures lower than those found in oil reservoirs. As temperature decreases, the temperature at which the saturated hydrocarbons begin to change phase from liquid to solid is referred to as the wax appearance temperature (WAT). In general, as the molecular weight of saturated hydrocarbons increases, the temperature at which saturated hydrocarbons come out of solution as solids increases (García and Urbina, 2003). The WAT is also determined by the breadth of distribution of paraffins, with wider distributions of carbon chain length resulting in a lower WAT (García, 2000; Roenningsen *et al.*, 1991; Vazquez and Mansoori, 2000). Significant changes to the physical properties of oils can occur below the WAT, and it is important to understand how these phase transitions influence the properties that determine acoustic scattering at oceanographically relevant temperature and pressures.

In this study a review of the measurements of sound speed available in the literature was performed and the results compared to Batzle and Wang (1992), a commonly used empirical model of the physical properties of oil. Samples of four crude oils were then chemically analyzed to quantify the concentration of saturated hydrocarbons and phase changes were identified and quantified by differential scanning calorimetry (DSC) over the relevant temperature range. To adequately characterize oils for acoustic scattering applications, the density and sound speed was measured over oceanographically relevant temperatures (−10 °C−30 °C). Sound speed was also measured at oceanographically relevant pressures (0–13.79 MPa). Finally, these results were also compared to the Batzle and Wang (1992) empirically derived model for sound speed and density of crude oils.

II. LITERATURE REVIEW

To evaluate the applicability of empirical models derived from measurements of oils at reservoir temperature and pressure to oceanographic conditions a literature review of available sound speed data was performed. Targeted search criteria returned 985 papers. These papers were further refined by exclusion criteria (Appendix A) designed to eliminate papers with insufficient data for modeling sound speed. For example, papers that did not include temperature and/or pressure of measurements were excluded. Following filtering by the exclusion criteria only nine papers made measurements of the sound speed of crude oil with sufficient data for modeling (Ball *et al.*, 2002; Bassett *et al.*, 2016; Chaudhuri *et al.*, 2012; Daridon *et al.*, 1998; George *et al.*, 2008; Han *et al.*, 2010; Khelladi *et al.*, 2010; Meng *et al.*, 2006; Plantier *et al.*, 2008). Of the measurements in those nine papers only 19.7% were made at oceanographically relevant temperatures and pressures. While models derived from reservoir temperatures and pressures may be relevant for oil exploration, the potential for phase changes in oils at lower temperatures and pressures limits the potential applicability of these models to oceanographically relevant conditions. The available literature also focuses primarily on

heavy oils; 70% of measurements at oceanographically conditions fell into this category.

In addition to the potentially limited applicability to oceanographic conditions, many of the available models and equations of state rely on *a priori* knowledge of a wide range of thermodynamic properties of oils (e.g., Gross and Sadowski, 2001). For oil spill responders and researchers, such thorough examinations of oil properties are often unfeasible due to the cost of characterization and limited access to large sample sizes. There are, however, simpler models that require fewer input parameters.

The most widely cited empirical model is Batzle and Wang (1992; hereafter referred to as BW92), which empirically derives values for the sound speed and density of oil based solely on API_g. Because the focus of BW92 was on reservoir conditions, the authors of BW92 limited their analysis of sound speed and density to data that do not include any phase transitions. Oil density as a function of pressure is determined in BW92 by

$$\rho_p = \rho_o + (0.00277P - 1.61 \times 10^{-7}P^3) \times (\rho_o - 1.15)^2 + 3.49 \times 10^{-4}P, \quad (1)$$

where ρ_p is the oil density in kg/m^3 at pressure P in MPa, ρ_o is the oil density at atmospheric pressure and 15.56 °C (API_g conditions). Temperature is accounted for according to

$$\rho_{P,T} = \frac{\rho_p}{\left[0.972 + 3.81 \times 10^{-4}(T + 17.78)^{1.175}\right]}, \quad (2)$$

where $\rho_{P,T}$ is the oil density as a function of pressure and temperature, T, in °C.

Figure 1 shows the residuals between BW92 and the sound speed data from seven of the nine papers (root-mean-square, RMS, error 96.0 m/s). Two of the nine papers (Daridon *et al.*, 1998; Khelladi *et al.*, 2010) did not have API_g or density data for the oils measured and therefore were excluded. BW92 overestimates the sound speed of light oils, RMS error = 211 m/s, underestimates medium and heavy oils, RMS error = 57 m/s and RMS error = 60 m/s, respectively. BW92 increasingly underestimates the sound speed of heavy oil as the temperature decreases.

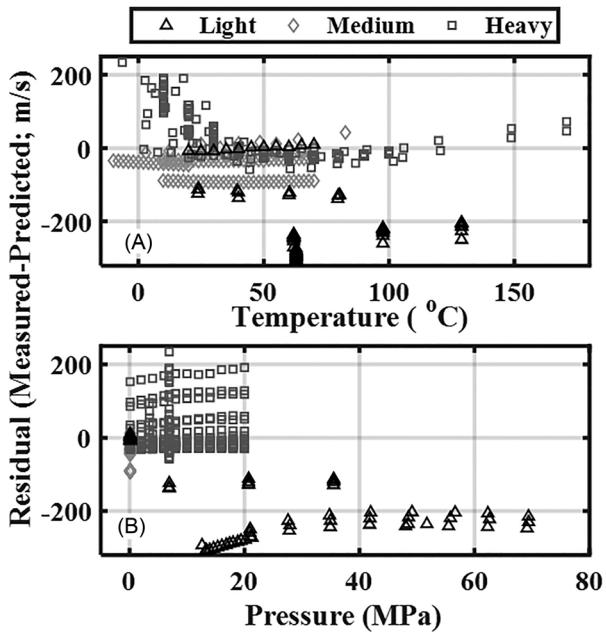

FIG. 1. Comparison of literature sound speed data and BW92 model as a function of (A) temperature and (B) pressure. Residuals are the difference between the literature sound speed and BW92 in m/s.

The heavy oil data from the literature show an exponential increase in sound speed at temperatures below 20 °C, which is not predicted by the BW92 model. Han *et al.* (2010) proposed that this exponential increase was due to a phase transition in the oil that they qualitatively referred to as the oil becoming "quasi-solid." The transition to quasi-solid state is presumably caused by the crystallization of waxes in the oils; however, the phase transition is not quantified by Han *et al.* (2010).

III. MATERIALS AND METHODS

Samples of four different crudes were obtained for analysis. The four oils studied are identified by the geographic region from which they were extracted: Alaskan North Slope ($API_g = 28.2°$), Coal Oil Point, Califonia ($API_g = 22.6°$), Angolan Bavuca ($API_g = 17.7°$), and Angolan Xikomba ($API_g = 24.4°$). The abbreviations ANS, COP, BAV, and XIK, respectively, will serve to reference the specific oils when discussing their properties. Based on their API gravities, ANS, COP, and XIK are all medium oils, while BAV is a heavy oil. All oils were analyzed for saturated hydrocarbon concentration and thermally characterized by DSC from −50 °C to 50 °C. Density was measured at ambient pressure for temperatures from −10 °C to 30 °C in 5 °C increments. Sound speed was also measured from −10 °C to 30 °C in 5 °C increments and at pressure from 0.10 MPa to 13.79 MPa in 3.45 MPa increments.

A. Calorimetry

DSC was performed on a TA Instruments DSC Q20 (New Castle, DE). DSC analysis reveals phase changes occurring within oil samples by measuring the heat flux required to change the temperature of a sample (Wunderlich, 1990). Deviations in the first derivative of the heat flux as a function of temperature in the test sample reveal the presence of a phase change over a temperature range. If the slope of heat flux as a function of temperature is constant over a region, no phase change is occurring. Measurements were performed by hermetically sealing each sample in an aluminum pan at atmospheric pressure. Samples were then heated to 50 °C, isothermed for 3 min, then cooled to −50 °C and isothermed again for 3 min. This was performed at 10 °C/min, 5 °C/min, and 3 °C/min.

B. Saturated hydrocarbons

Saturated hydrocarbon analysis (SHC) was performed by Alpha Analytical (Westborough, MA) according to EPA SW-846 method 8015D (US EPA, 2007). This method uses gas chromatography with flame ionization detector (GC/FID) to determine the concentration of 32 *n*-alkane

hydrocarbons (saturated hydrocarbons with only single covalent bonds) and selected isoprenoids for carbon chains from 9 carbons to 40 carbons in length. The method also reports the total concentration of saturated hydrocarbons along with the total petroleum hydrocarbons.

C. Density

Density was measured by calibrated hydrometers, FisherSci 11510B and 11510C (Waltham, MA), according to ASTM D1298-12b (ASTM, 2017). Approximately 250 mL of each was oil transferred at room temperature into 300 mL ungraduated cylinders and sealed with parafilm. The sealed cylinders and hydrometers were placed in a temperature-controlled incubator, ESPEC BTL-433 (Hudsonville, MI), which was set to −10 °C. A National Institute of Standards and Technology (NIST) certified Omega Ultra Precise Platinum RTD (resistance temperature detector) temperature probe (PMA-1/8-6-1/2-TS5, Norwalk, CT; range: −100 °C−250 °C, accuracy: 0.15 °C±0.002|T|, where T is the temperature of measurement) connected to a NIST certified Omega High Accuracy PT100 Input Thermometer (HH804U; accuracy 0.05%|T|) was inserted through the parafilm into the XIK sample, which had the highest heat capacity over the temperature range as measured by DSC. Once the incubator temperature was stable, the samples were given 1.5 h to equilibrate. XIK reached a stable temperature of −9.8 °C after 45 min. Samples then sat for an additional 45 min to assure that the entire sample reached equilibrium. Temperature inside the incubator was constantly recorded by an RBR solo T Temperature Logger (Ottawa, ON, Canada, accuracy ±0.002 °C) recording at a 1-s sample rate. Hydrometers were placed in each sample and allowed to equilibrate for 30 min. Each hydrometer was read and recorded, noting the maximum height of the oil on the hydrometer. Corrections for opaque liquid meniscus and glass expansion/contraction were made according to ASTM D1298–12b (ASTM, 2017). The temperature of the chamber was then set to −5 °C and once the temperature in the chamber was stable, the samples were allowed 1 h to equilibrate. These steps were repeated to obtain measurements in 5 °C intervals from −10 °C to 30 °C.

D. Sound speed

Sound speed measurements were made using a system modified from the design by Dashti and Riazi (2014). The chamber was vacuum filled to minimize air entrainment in the sample. Sound was generated by a piezoelectric transducer held in the center of two cylindrical stainless-steel chambers (Fig. 2). The transducer was driven by an Agilent Arbitrary Waveform Generator (Santa Clara, CA), which drives a 10-V peak-to-peak, five-cycle, 750-kHz pulse that travels bi-directionally through the length of each chamber. No tapering window was applied to the signal. The waves are reflected by the end caps and then return to the transducer. A Tektronix TBS 1102B Digital Oscilloscope (Portland, OR) records the voltages associated with the reflected waves. Data were recorded over a 100-μs window encompassing only the first and second returns (excluding the transmit pulse and higher multiple returns) with a sample

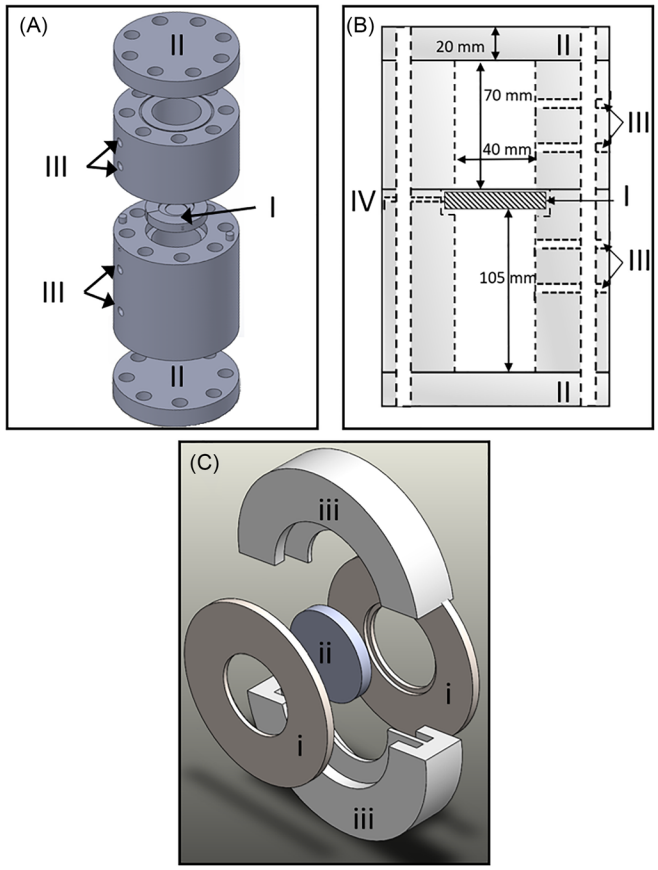

FIG. 2. (Color online) (A) Exploded exterior view of sound speed chamber with (I) The piezoelectric sandwich, (II) the endcaps, and (III) the fill and pressure ports. (B) Cross-sectional view of interior of sound speed chamber with same labeling as (A) with the addition of (IV) the hole through which the wires to the piezoelectric "sandwich" pass. (C) The piezoelectric sandwich. The brass washers (i) are wired to the signal generator with one washer wired to positive and the other to negative. These washers sit flush against the face of the piezoelectric transducer (ii). The washers and held apart and the entire sandwich held together by the plastic spacers (iii), which also fit flush against the inside of the sound speed chamber.

rate of 2.5 MHz. The Tektronix TBS 1102B Digital Oscilloscope records 16 individual wave forms, coherently averages them together to reduce noise and outputs that average as a single waveform. For a given temperature and pressure 100 of the outputted waveforms were recorded.

Figure 3 diagrams the environmental control and data recording setup for sound speed measurements. The internal pressure of the system was controlled by a precision pressure control valve connected to a scuba tank. Pressure data were recorded by a NIST certified Omega Digital Pressure Gauge (DPG409–3.5 KG, Norwalk, CT) with and accuracy of 0.08% of the full scale (24 MPa). Temperature was controlled by placing the chamber in an insulated polyvinyl chloride (PVC) housing connected to a PolyScience Programmable Temperature Controller (Warrington, PA). A 50/50 mixture of water/ethylene glycol was used as the bath fluid to permit temperatures as low as −50 °C. Temperature in the housing was recorded by a NIST certified Omega Ultra Precise Platinum RTD temperature probe (PMA-1/8-6-1/2-TS5) connected to a NIST certified Omega High Accuracy PT100 Input Thermometer (HH804U). Data recorded by the oscilloscope were recorded in MATLAB.

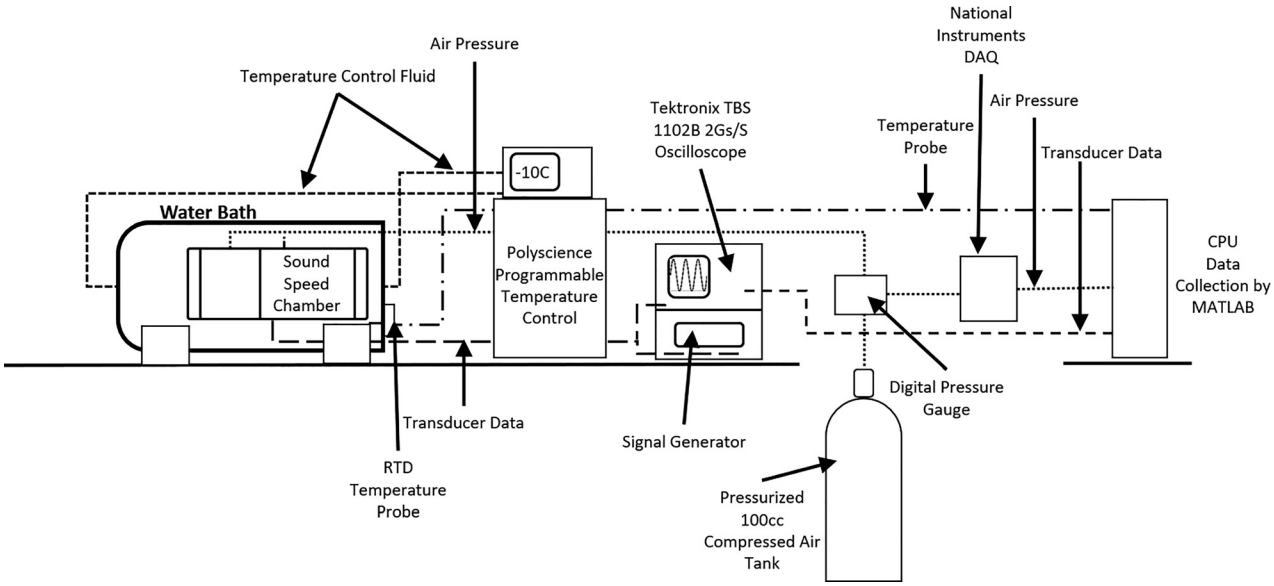

FIG. 3. Diagram of sound speed chamber temperature and pressure control and data collection.

During temperature transitions, MATLAB was used to calculate real-time sound speed using a single recorded waveform every 10 s. When the sound speed was constant (not changing by more than 0.1 m/s) over a 10-min period, it was determined that the oil had reached equilibrium with the fluid bath.

The path length difference between the two sides of the sound speed chamber was calibrated using ASTM type 1 deionized (DI) water, as detailed in Appendix B. The calibration evaluated the effects of temperature and pressure on the path lengths and found that there was no significant relationship between the estimates of $\Delta\ell$, the difference in path length between the sides of the chamber, and temperature, pressure, or both. The mean path length difference for all temperatures and pressures is 69.934 mm ± 0.245 mm (95% confidence interval, CI). For a 1500 m/s fluid this equates to an uncertainty in sound speed of ±5.3 m/s.

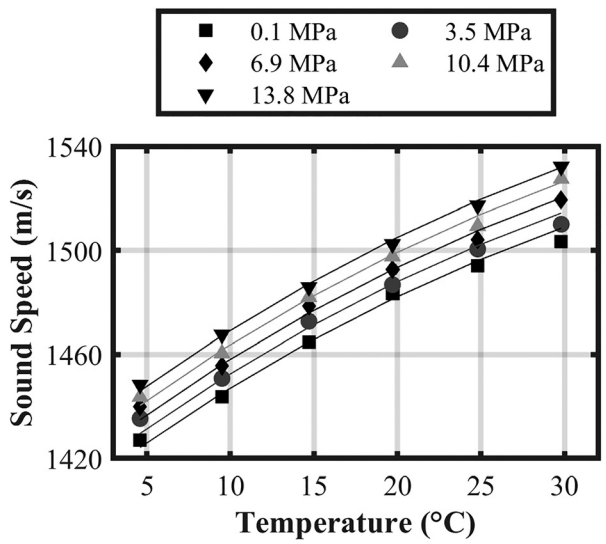

FIG. 4. Sound speed of type 1 DI water measured (markers) compared to Belogol'skii *et al.* (1999; lines).

Sound speed, c, is calculated by dividing the mean path length difference by the difference in arrival time for the two waves according to

$$c = \Delta\ell/\Delta t, \tag{3}$$

where the propagated uncertainty for σ_c was calculated according to

$$\sigma_c = \pm c\sqrt{\left(\frac{\sigma_\ell}{\ell}\right)^2 + \left(\frac{\sigma_{\Delta t}}{\Delta t}\right)^2}, \tag{4}$$

where σ_ℓ and $\sigma_{\Delta t}$, are the standard deviations of the length and time difference, respectively. The 95% CIs of all sound speed measurements was between 5.0 m/s and 5.4 m/s. Results agree well with the Belogol'skii *et al.* (1999) model for pure water (RMS error 2.5 m/s, Fig. 4).

Equation (3) was used to calculate sound speed for ANS, XIK, BAV, and COP, using the temperature and pressure independent estimate of $\Delta\ell$ from the DI water calibration corrected for thermal expansion at the temperature of a given measurement.

IV. RESULTS AND DISCUSSION

A. Calorimetry

DSC results are summarized in Table I. DSC did not detect any phase changes in BAV over the measurement

TABLE I. Phase transition and percent saturation for four crude oils. Phase transition data are from DSC analysis. Percent saturation was determined by SHC.

	ANS	XIK	COP	BAV
Enthalpy (J/g)	0.58	3.26	4.70	n/a
Onset of melt (°C)	−13.7	−18.3	−40.9	n/a
Peak melt temperature (°C)	3.08	7.62	−11.19	n/a
Wax appearance temperature (°C)	14.68	20.66	19.60	n/a
Percent saturation (%)	11.2	16.5	13.1	0.8

range, but did detect phase change in ANS, XIK, and COP. Enthalpy is the integrative measure of the magnitude of a phase transition and was the highest for COP and lowest for ANS. The phase transition is bounded by the WAT (the temperature at which waxes begin to form) and the onset of melt (the value below which no more waxes are solidifying). Peak melt temperature is the temperature at which enthalpy is greatest in the transition. While COP has a higher overall enthalpy, the majority of its phase transition occurs below the oceanographically relevant range. XIK has the next highest enthalpy, and its phase transition occurs over almost the entire measurement range. ANS has a much lower enthalpy, and while the transition is within the measurement range, the overall magnitude of the transition is much smaller than XIK and COP.

B. Saturated hydrocarbons

XIK has the highest concentration of saturated hydrocarbons, relative to total petroleum hydrocarbons, followed by COP, ANS, and BAV (Table I). When comparing this data to the DSC results above, oils that have a phase transition have higher percent saturation, the ratio of saturated hydrocarbons to all hydrocarbons. XIK has the highest total saturated hydrocarbon concentration at all molecular weights (Fig. 5). This broad distribution of saturated hydrocarbons and higher concentration of longer chain waxes results in the higher enthalpy. While COP has a high concentration of saturated hydrocarbons, the concentration of high molecular weight paraffins is lower than XIK, contributing to the lower phase transition temperature. ANS has a lower percent saturation, and fewer long chain saturated hydrocarbons contributing to the lower total enthalpy. Since BAV only has a small number of low molecular weight paraffins, it possesses a weak phase transition at very low temperatures.

C. Density

All oils have an inverse relationship between temperature and density (Fig. 6). BAV, COP, and ANS all have similar relationships between temperature and density, regardless of the presence of a phase transition as detected by DSC. Below the WAT, XIK transitioned from liquid to higher

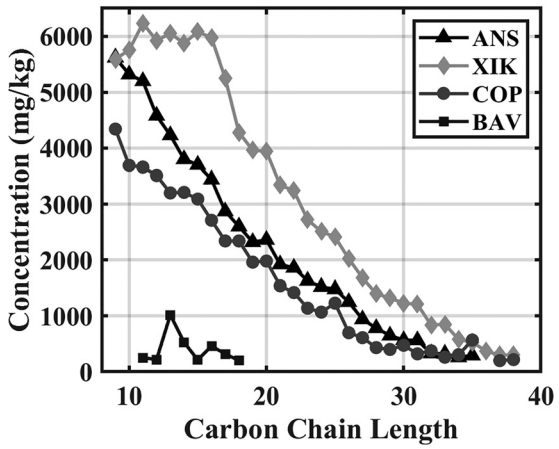

FIG. 5. Concentration of saturated hydrocarbons by carbon chain length.

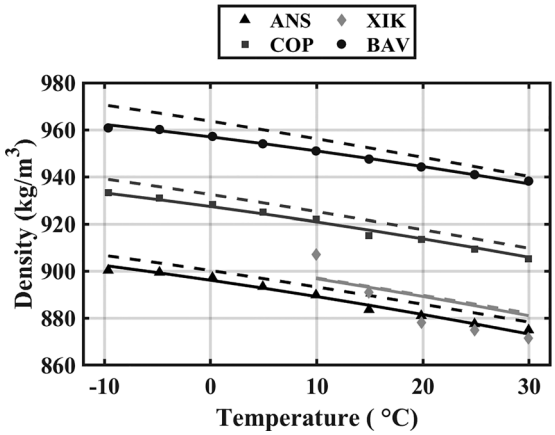

FIG. 6. Density results comparing measured (markers), empirically derived model in this study (solid lines) and BW92 (dashed lines).

density waxy solid with an increasingly rapid rise in density with decreasing temperature. Below the peak melt temperature the viscosity of XIK was too high for measurements of density to be made (the hydrometer was effectively stuck in place).

API_g for use in the BW92 model was calculated by fitting a second-order polynomial to the data to get the density at 15.5 °C. BW92 slightly overpredicts the density for all oils (Fig. 6), except for XIK at 10 °C, where BW92 underpredicts density. The RMS error for the BW92 model for all oils is 25.9 kg/m^3.

To improve on BW92, an empirically fit model was developed. A stepwise regression was computed using input parameters API_g and temperature. Coefficients were calculated for both input parameters as well as linear and quadratic combinations of these parameters. Any input parameters or combinations with correlation p-values less than 0.05 were rejected (Draper and Smith, 1998). XIK was excluded from the modeling analysis: in order to accurately model the relationship between density and temperature for oils with a significant phase transition similar to that seen for XIK would require more than two measurements below the phase transition temperature. Therefore, this empirically derived model is applicable only to oils with either no phase transition over the modeled range (BAV) or a very weak transition over the modeled range (ANS and COP). The result is a six-term equation for the density of crude oil as a function of temperature with inputs ρ_0, density (kg/m^3) at API conditions (15.56 °C and 0.1 MPa), and T, the temperature in °C,

$$\rho = C_0 + C_1 T + C_2 \rho_o + C_3 T \rho_o + C_4 T^2 + C_5 \rho_o^2, \qquad (5)$$

with coefficients in Table II.

The new model has RMS error equal to 2.0 kg/m^3, including XIK (1.1 kg/m^3, excluding XIK).

D. Sound speed

Sound speed decreases with increasing temperature and decreasing pressure. The three medium oils all have similar sound speeds, while BAV has a sound speed on the order of

TABLE II. Coefficients for empirically derived model in this study for density and sound speed.

Coefficient	Density	Sound speed
C_0	−995.02	2148.4
C_1	−2.011	−4.1630
C_2	3.249	3.548
C_3	1.527×10^{-3}	−50.25
C_4	-3.405×10^{-3}	2.0402×10^{-2}
C_5	-1.255×10^{-3}	8.7438×10^{-3}
C_6	—	0.95175

75 m/s higher for all temperature and pressures (Fig. 7). At 5 °C BAV showed exceptionally high signal attenuation to the point that there was no detection from the longer side of the chamber and a very low amplitude signal from the short side. Below 5 °C no echoes were detected. Due to the low signal-to-noise ratio, no reliable measurements of sound speed were possible below 10 °C for BAV.

BW92 predicts significant deviations from the measured sound speeds, RMS error 42.5 m/s, and largest magnitude residual −74.6 m/s (Fig. 8). A new empirical model was derived using a stepwise regression analysis. Regression coefficients were calculated for all input parameters (temperature, sound speed, and API_g) as well as all linear and quadratic combinations of parameters. Any coefficients with regression p-values greater than 0.05 were excluded. The result is a seven-term model with inputs T, temperature in °C, P, pressure in MPa, and API_g,

$$c = C_0 + C_1T + C_2P + C_3\mathrm{API} + C_4TP + C_5T^2 + C_6\mathrm{API}^2, \quad (6)$$

with coefficients listed in Table II. The RMS error for the new model is 7.4 m/s with maximum residual 28.2 m/s (Fig. 8). This empirical model provides a better fit than BW92 over oceanographically relevant temperatures and pressures while still only including temperature, pressure, and API_g as input parameters.

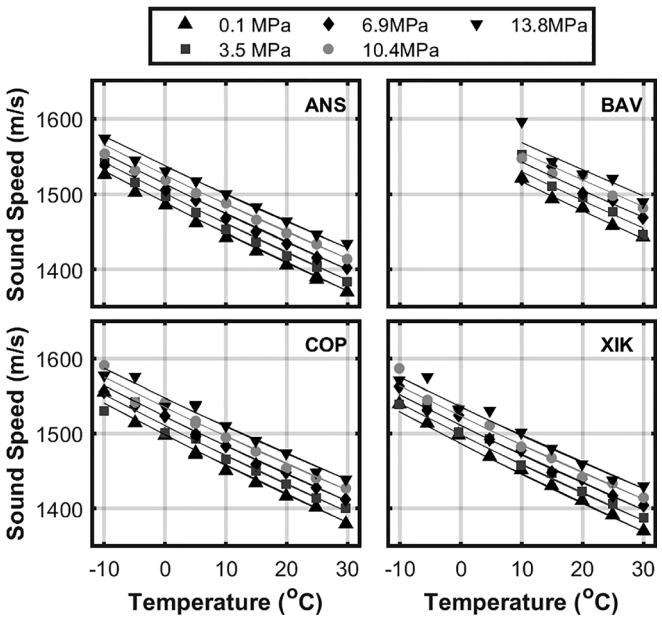

FIG. 7. Measured sound speed (markers) and empirically derived model from this study (lines).

The empirical model derived in this study was compared to literature values for oceanographically relevant temperatures and pressures. The new empirical model is a marginally better predictor of sound speed for literature data, RMS error 76.3 m/s compared to 84.9 m/s for BW92. The literature data include three measurements of light oils whose API gravities are much higher than the oils analyzed here (two measurements of API_g 37.7° and one of 45.6°). The empirical model derived here is a poor predictor of sound speed for light oils due to lack of light oil measurements. If the three measurements of light oils are removed from both BW92 and the new empirical model, the RMS error for the new model improves to 55.1 m/s, while BW92 RMS error stays relatively unchanged at 85.2 m/s. For medium and heavy oils, the new empirical model is a better predictor of sound speed (Fig. 9).

E. Implications for scattering models

The broadband acoustic backscatter from a 2 mm radius spherical COP droplet at 15 °C and ambient pressure (0.1 MPa) is analyzed here as an illustrative example of the importance of well-constrained acoustic properties. A wide range of frequencies are used to detect and quantify oil from shipboard instruments in the 100s of kHz range to MHz imagining sonars. The example here focuses on the lower, shipboard frequencies. The sound speed for COP oil measured in this study at 15 °C and 0.1 MPa is 1434.3 ± 5.03 m/s. Using the empirically derived model in this study, the sound speed is 1438.4 ± 14.8 m/s, while the BW92 model provides a sound speed of 1491.9 ± 85 m/s. The density of COP measured in this study at these same conditions is 915.0 kg/m^3, for the empirical model in this study the density is predicted to be 917.4 ± 2.24 kg/m^3 and the empirical BW92 model predicts 921.5 ± 12.0 kg/m^3. Figure 10 shows the results of the Anderson (1950) scattering model for a 2-mm radius spherical droplet using the three different acoustic impedances—measured in this study, predicted by the empirical model derived in this study and according to the BW92 empirical model. The surrounding medium was assumed to be seawater with density = 1026 kg/m^3 and sound speed 1473 m/s. The newly derived model is a better predictor of the peak target strength (TS), as well as the frequency range of the null, two important factors for inverting scattering models to predict droplet properties.

Another example of the importance of well-constrained acoustic properties is in modeling the reflection of sound generated in the water column and reflected from oil layers. Such scattering is most accurately modeled as a three-layer problem, however, for brevity and simplicity it is modeled here as a two layer-problem where the oil and water both occupy a half space. When the interface between the fluids is acoustically smooth, the reflected energy is a function of the mismatch in the acoustic impedance. As the difference in acoustic impedance across the water–oil interface approaches zero, little energy is reflected. At oceanographically relevant

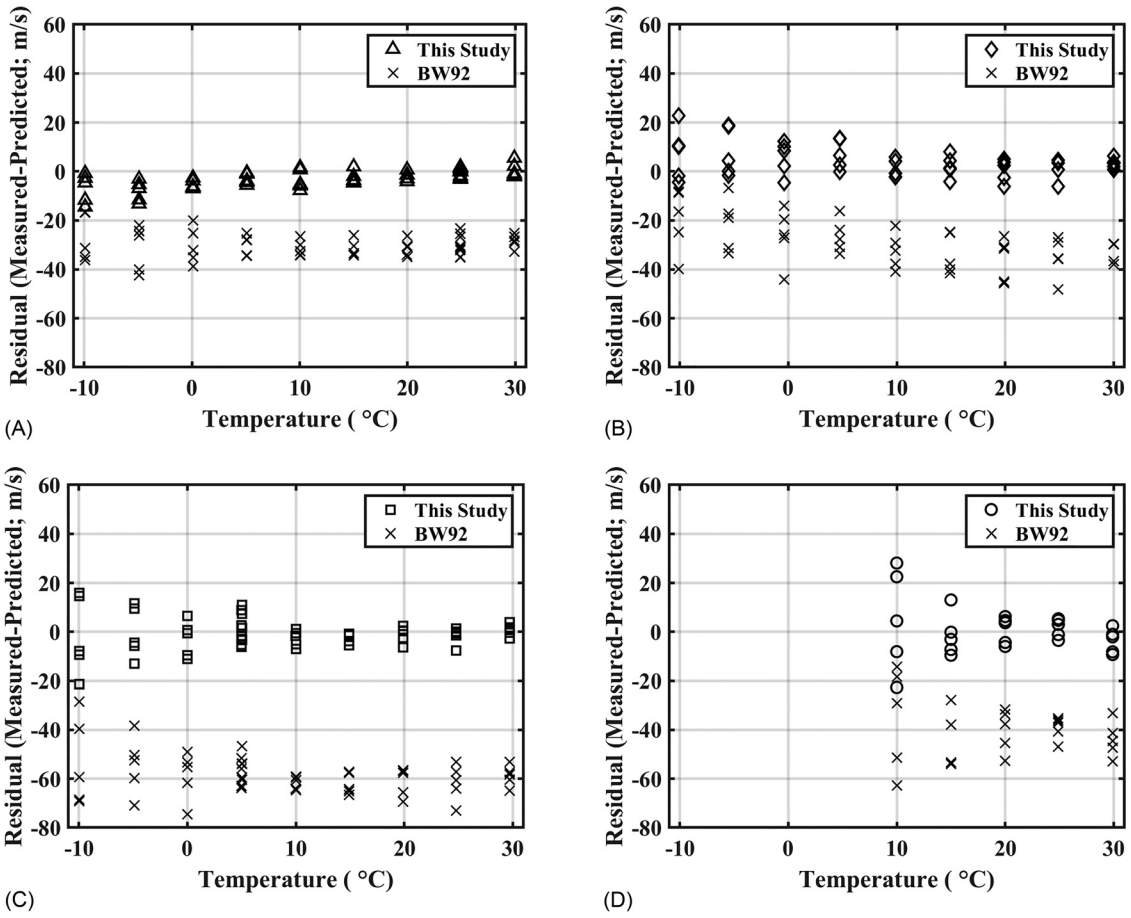

FIG. 8. Residuals for sound speed measured in the present work and newly derived model compared to residuals for sound speed measured in the present work and BW92. (A) ANS, (B) XIK, (C) COP, (D) BAV.

temperatures and pressure, the conditions under which the detection of oil layers is difficult depends on the acoustic properties of both the water and oil. Figure 11 shows modeled reflection coefficients from an acoustically smooth water–oil interface over a range of API gravities and water temperatures. Modeled oil temperatures are at equilibrium with the water. Local minima occur from −2 °C to 15 °C for oils with API gravities between 15° and 37°. Notably, at the lowest modeled temperatures when conditions would be consistent with an oil layer under ice, light and heavy oils would be more difficult to detect than medium oils. The minima for medium oil occurs at higher temperatures, up to 12 °C, and is mostly likely to occur for oil at the sea surface when ice is not present. In the case of a three-medium problem, the oil-water layer would effectively disappear, and reflection would occur from the fluid–ice or fluid–atmosphere interface. These results demonstrate the importance of adequately constrained acoustic properties when setting

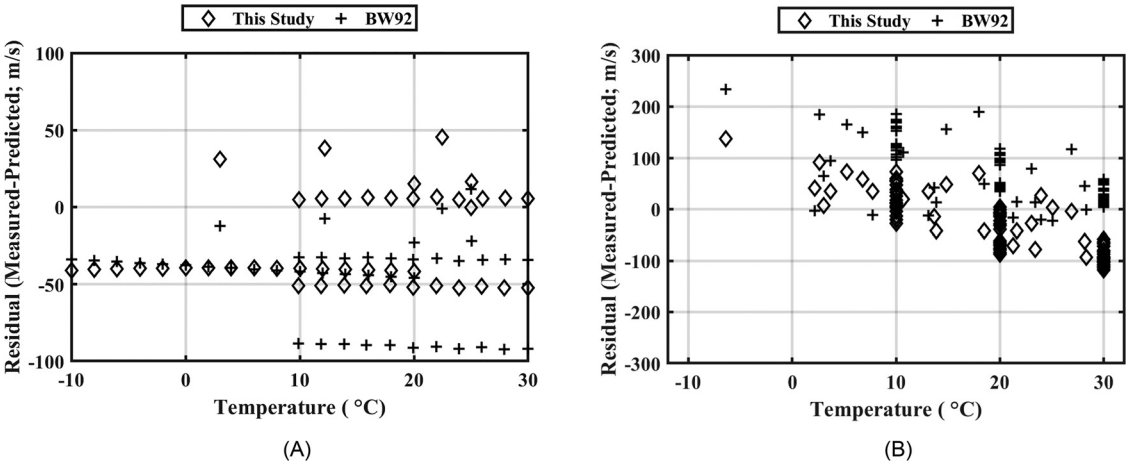

FIG. 9. Residuals between literature values for sound speed and the empirical equation from this study as well as BW92. (A) Medium oil, (B) heavy oil.

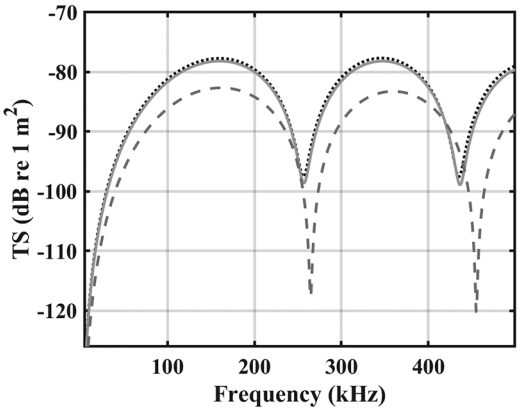

FIG. 10. Acoustic scattering predicted by Anderson (1950) using the measured impedance (dotted line), impedance predicted by BW92 (dashed), and impedance predicted by the empirically derived model in this study (solid line) for a COP droplet at 25 °C.

thresholds for detecting and quantifying crude oil in ocean environments.

V. CONCLUSIONS

The empirical models derived in this study are limited in sound speed to medium and heavy oils, and in density to oils that do not have a large phase transition in the temperature range. More data are need, including phase transition information, in order to expand this model and determine its applicability to light oils and oils where waxes become solid over the range of interest.

Active acoustic measurements are a powerful tool that can be used along with other techniques to detect and quantify oil in oceanographic applications. While acoustic scattering techniques may be used to detect oil droplets or oil layers without *a priori* knowledge of the acoustic properties of the oil, quantification of volumes in oil layers and fluxes associated with oil droplets is contingent upon acoustic properties that are adequately constrained. Complex models requiring a wide range of physical and thermodynamic oil properties as inputs may improve accuracy; however, researchers and oil spill responders often do not have the time or sample volume to obtain a wide range of properties. We propose a simpler empirical model, requiring only the API_g and environmental conditions (temperature and pressure) to predict density and sound speed at environmental conditions relevant to oil in the ocean. Our model shows significant improvement over the relevant environmental conditions compared to BW92, which was derived from conditions relevant to oil in subsurface reservoirs. When direct measurements of sound speed and density are unavailable, this empirical model can be used to improve the accuracy of predictions of acoustic scattering used to estimate oil flux in the water column and oil layer thickness, both of which are crucial to determining the natural background levels of hydrocarbons in the environment and the environmental impact of anthropogenic spills.

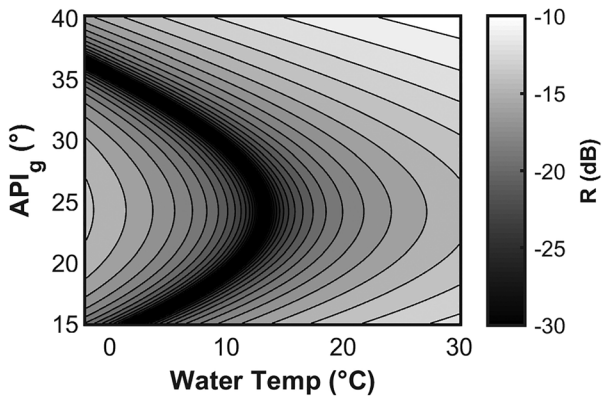

FIG. 11. Reflection coefficients for an acoustically smooth water–oil interface as a function of API gravity and temperature assuming that the oil and water temperatures are at equilibrium (Clay and Medwin, 1977). The acoustic properties of the oil are determined by the empirically derived model [Eqs. (5) and (6)] at atmospheric pressure and the water has a salinity of 30 psu. Local minima in the reflection coefficient curve highlight the combinations of oil and water properties that would make the detection of thin oil layers difficult using acoustic scattering techniques.

The literature review provided examples of where heavy oils showed an exponential increase in sound speed at low temperatures due to what was qualitatively described as a transition to a quasi-solid state (Han *et al.*, 2010). By contrast, the present study found that solidification of waxes can occur in medium oils, but that phase transition did not significantly impact the sound speed as a function of temperature over the range studied here. However, the present study focused on a relatively narrow temperature range and it may be the case that the sound speed changes exponentially with temperature over a broader range. The empirical model derived here is more applicable to oceanographically relevant conditions than a model derived from higher temperature and pressure measurements. More samples of heavy, medium, and light crudes that show solid wax formation over the relevant temperature range are needed to fully determine how this transition affects sound speed and model how the transition impacts density.

ACKNOWLEDGMENTS

We thank Alpha Analytical Environmental Testing Laboratory for providing the SHC; John Mousette from JW Precision Co. Inc. and Paul Lavoie from University of New Hampshire for fabrication of the sound speed chamber; Peter Vrolijk and John Blum from Exxon Mobile and David Valentine from University of California Santa Barbara for providing the crude oil samples. The work was supported by the National Oceanic and Atmospheric Administration (Grant No. NA15NOS4000200). The scientific results and conclusions, as well as any views or opinions expressed herein, are those of the author(s) and do not necessarily reflect the views of NOAA or the Department of Commerce. Reference to trade names does not imply endorsement by the National Marine Fisheries Service, NOAA.

APPENDIX A: LITERATURE REVIEW

A review of primary scientific literature was performed using the Web of Science database using the following terms: “sound speed” OR “speed of sound” OR

"sound velocity" OR "velocity of sound" OR "wave velocity" OR "wave speed" OR "seismic properties") AND (Oil OR Hydrocarbons OR Crude OR Petroleum OR "pore fluid"). These keywords were designed to capture any study that either directly measures, or uses other physical parameters to determine, the speed of sound in crude oil, as well as any models for the sound speed of oil based on other physical properties. The search returned an initial pool of 985 papers. These papers were screened for relevance to the topic of interest. Papers were then screened and excluded if:

(1) They did not contain measurements of sound speed or derivation of sound speed from other physical properties.
(2) Sound speed measurements were not associated with a density, API_g or API_g based classification (light, medium, heavy, or extra heavy).
(3) Experiments were performed using hydrocarbons not derived from or composed of crude petroleum.
(4) Mineral oils were excluded.
(5) The same data were used in multiple papers. In this case only the earliest publication of those same results was recorded.
(6) They were not studies of hydrocarbon mixtures of greater than three different length hydrocarbon chains.
(7) Papers did not include either temperature or pressure data.
(8) They did not report sufficient data for inclusion in analysis.
(9) Oil-in-water mixtures were excluded.
(10) Seismic studies were excluded.

APPENDIX B: SOUND SPEED CHAMBER DI WATER CALIBRATION

The sound speed chamber was calibration using ASTM type I DI water. Sound speed measurements were made at 5 °C increments from 5 °C to 30 °C and 3.4 MPa increments from 0.1 MPa to 13.8 MPa. Each recorded time series from the transducer was filtered using a fifth-order Butterworth bandpass filter to decrease out-of-band noise.

Analytical forms of each waveform were then normalized to their peak value and autocorrelated (Fig. 12). The difference in time between the peak of the correlation from the echo from the shorter side (t_1) and the peak of the correlation from the longer side (t_2) gives the difference in time-of-flight for each pressure and temperature, $\Delta t_{T,P}$, for the two chambers ($\Delta t_{T,P} = t_2 - t_1$). The sound speed of distilled water, c_{ref}, was modeled according to Belogol'skii *et al.* (1999) and was used to calculate the difference in path length between the two sides of the chamber for each temperature and pressure according to

$$\Delta \ell'_{P,T} = c_{\text{ref}}(\Delta t_{P,T}). \tag{B1}$$

Each difference in path length is then corrected for the difference in length of each section of the chamber caused by thermal expansion,

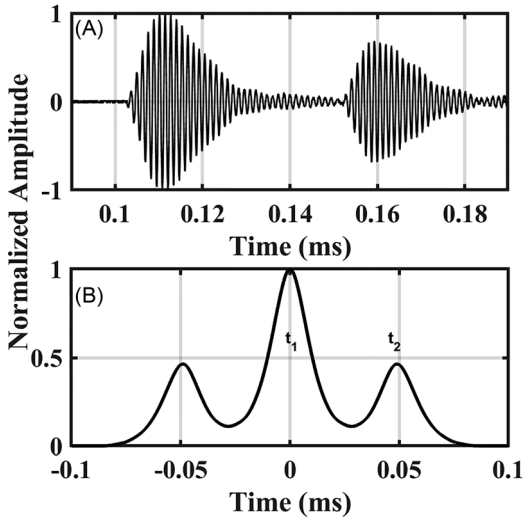

FIG. 12. (A) Raw waveform showing the return from the shorter side and the lower amplitude return from the second side. (B) Autocorrelation of (A) with times used to calculate sound speed labeled.

$$\Delta \ell_{P,T} = \Delta \ell'_{P,T} - 2\ell_2 \boldsymbol{\alpha_L}(T-23) - 2\ell_1 \boldsymbol{\alpha_L}(T-23), \tag{B2}$$

where $\ell_2 = 110$ mm is the length of the longer chamber at 23 °C according to the design, $\ell_1 = 70$ mm is the length of the shorter chamber at 23 °C according to the design and $\boldsymbol{\alpha_L} = 16.6 \times 10^{-6}$ m/m/K is the coefficient of thermal linear expansion for stainless steel (ASTM, 2017). The estimates of $\Delta \ell_{P,T}$ were then regressed against temperature, pressure, and temperature and pressure combined.

Anderson, V. (**1950**). "Sound scattering from a fluid sphere," J. Acoust. Soc. Am. **22**(4), 426–431.
ASTM (**2017**). A276-98b, *Standard Specification for Stainless Steel Bars and Shapes* ASTM Standard A582/A582M (American Society for Testing and Materials, Philadelphia).
Ball, S. J., Goodwin, A. R. H., and Trusler, J. P. M. (**2002**). "Phase behavior and physical properties of petroleum reservoir fluids from acoustic measurements," J. Pet. Sci. Eng. **34**(1-4), 1–11.
Bassett, C., Lavery, A. C., Maksym, T., and Wilkinson, J. P. (**2016**). "Broadband acoustic backscatter from crude oil under laboratory-grown sea ice," J. Acoust. Soc. Am. **140**(4), 2274–2287.
Batzle, M., and Wang, Z. (**1992**). "Seismic properties of pore fluids," Geophysics **57**(11), 1396–1408.
Belogol'skii, V., Sekoyan, S., Samorukova, L., Stefanov, S., and Levtsov, V. (**1999**). "Pressure dependence of the sound velocity in distilled water," Meas. Tech. **42**(4), 406–413.
Camilli, R., Di Iorio, D., Bowen, A., Reddy, C. M., Techet, A. H., Yoerger, D. R., Whitcomb, L. L., Seewald, J. S., Sylva, S. P., and Fenwick, J. (**2012**). "Acoustic measurement of the Deepwater Horizon Macondo well flow rate," Proc. Natl. Acad. Sci. U.S.A. **109**(50), 20235–20239.
Chaudhuri, A., Osterhoudt, C., and Sinha, D. (**2012**). "An algorithm for determining volume fractions in two-phase liquid flows by measuring sound speed," J. Fluids Eng. **134**(10), 101301.
Clay, C., and Medwin, H. (**1977**). *Acoustical Oceanography: Principles and Applications* (Wiley, New York).
Crooke, E., Talukder, A., Ross, A., Trefry, C., Caruso, M., Carragher, P., Stalvies, C., and Armand, S. (**2015**). "Determination of sea-floor seepage locations in the Mississippi Canyon," Mar. Pet. Geol. **59**, 129–135.
Daridon, J. L., Lagourette, B., Xans, P., and Montel, F. (**1998**). "Petroleum characterization from ultrasonic measurement," J. Petr. Sci. Eng. **19**, 281–293.
Dashti, H. H., and Riazi, M. R. (**2014**). "Acoustic velocities in petroleum fluids: Measurement and prediction," J. Pet. Sci. Eng. **124**, 94–104.
Draper, N. R., and Smith, H. (**1998**). *Applied Regression Analysis*, 3rd ed. (Wiley, New York), pp. 307–312.

García, M. d. C. (**2000**). "Crude oil wax crystallization. The effect of heavy *n*-paraffins and flocculated asphaltenes," Energy Fuels **14**(5), 1043–1048.
García, M. d. C., and Urbina, A. (**2003**). "Effect of crude oil composition and blending on flowing properties," Pet. Sci. Technol. **21**(5–6), 863–878.
George, A. K., Al-Majrafi, N., Singh, R. N., and Arafin, S. (**2008**). "Thermo-elastic and thermodynamic properties of light and heavy crude oil," Phys. Chem. Liq. **46**(3), 328–341.
Greinert, J., Artemov, Y., Egorov, V., De Batist, M., and McGinnis, D. (**2006**). "1300-m-high rising bubbles from mud volcanoes at 2080 m in the Black Sea: Hydroacoustic characteristics and temporal variability," Earth Planet. Sci. Lett. **244**(1–2), 1–15.
Gross, J., and Sadowski, G. (**2001**). "Perturbed-chain SAFT: An equation of state based on a perturbation theory for chain molecules," Ind. Eng. Chem. Res. **40**(4), 1244–1260.
Han, D.-h., Liu, J., and Batzle, M. (**2010**). "Seismic properties of heavy oils—Measured data," in *Heavy Oils: Reservoir Characterization and Production Monitoring*, edited by S. Chopra, L. R. Lines, D. R. Schmitt, and M. L. Batzle (Society of Exploration Geophysicists, Tulsa, OK), Chap. 2, pp. 73–80.
Heeschen, K. U., Tréhu, A. M., Collier, R. W., Suess, E., and Rehder, G. (**2003**). "Distribution and height of methane bubble plumes on the Cascadia Margin characterized by acoustic imaging," Geophys. Res. Lett. **30**(12), 1643, https://doi.org/10.1029/2003GL016974.
IHS Markit (**2015**). "Offshore rig data: Weekly rig count: IHS petrodata," available at https://ihsmarkit.com/products/offshore-oil-rig-data.html (Last viewed June 1, 2018).
Jatiault, R., Dhont, D., Loncke, L., de Madron, X. D., Dubucq, D., Channelliere, C., and Bourrin, F. (**2018**). "Deflection of natural oil droplets through the water column in deep-water environments: The case of the Lower Congo Basin," Deep Sea Res., Part I **136**, 44–61.
Judd, A. G. (**2003**). "The global importance and context of methane escape from the seabed," Geo-Mar. Lett. **23**(3–4), 147–154.
Khelladi, H., Plantier, F., and Daridon, J. L. (**2010**). "A phase comparison technique for sound velocity measurement in strongly dissipative liquids under pressure.," J. Acoust. Soc. Am. **128**(2), 672–678.
Kvenvolden, K. A., and Cooper, C. K. (**2003**). "Natural seepage of crude oil into the marine environment," Geo-Mar. Lett. **23**(3–4), 140–146.
Meng, G., Jaworski, A. J., and White, N. M. (**2006**). "Composition measurements of crude oil and process water emulsions using thick-film ultrasonic transducers," Chem. Eng. Process. Process Intensif. **45**(5), 383–391.
Merewether, R., Olsson, M. S., and Lonsdale, P. (**1985**). "Acoustically detected hydrocarbon plumes rising from 2-km depths in Guaymas Basin, Gulf of California," J. Geophys. Res. **90**(B4), 3075–3085, https://doi.org/10.1029/JB090iB04p03075
Pegau, S., Garron, J., Zabilansky, L., Bassett, C., Bello, J., Bradford, J., Carns, R., Courville, Z., Eicken, H., Elder, B., Eriksen, P., Lavery, A., Light, B., Maksym, T., Marshall, H., Oggier, M., Perovich, D., Pacwiardowski, P., Singh, H., Tang, D., Wiggins, C., and Wilkinson, J. (**2017**). "Detection of oil in and under ice," Int. Oil Spill Conf. Proc. **2017**(1), 1857–1876.
Plantier, F., Bessières, D., Daridon, J. L., and Montel, F. (**2008**). "Structure and thermodynamic consistency of heavy oils: A study on the basis of acoustic measurements," Fuel **87**(2), 196–201.
Roberts, H. H., and Carney, R. S. (**1997**). "Evidence of episodic fluid, gas, and sediment venting on the northern Gulf of Mexico continental slope," Econ. Geol. **92**(7–8), 863–879.
Roenningsen, H. P., Bjoerndal, B., Hansen, A. B., and Pedersen, W. B. (**1991**). "Wax precipitation from north sea crude oils. 1. Crystallization and dissolution temperatures, and Newtonian and non-Newtonian flow properties," Energy Fuels **5**(6), 895–908.
Römer, M., Sahling, H., Pape, T., Bohrmann, G., and Spieß, V. (**2012**). "Quantification of gas bubble emissions from submarine hydrocarbon seeps at the Makran continental margin (offshore Pakistan)," J. Geophys. Res. **117**, C10015, https://doi.org/10.1029/2011JC007424.
Sahling, H., Borowski, C., Escobar-Briones, E., Gaytán-Caballero, A., Hsu, C.-W., Loher, M., MacDonald, I., Marcon, Y., Pape, T., Römer, M., Rubin-Blum, M., Schubotz, F., Smrzka, D., Wegener, G., and Bohrmann, G. (**2016**). "Massive asphalt deposits, oil seepage, and gas venting support abundant chemosynthetic communities at the Campeche Knolls, southern Gulf of Mexico," Biogeosciences **13**, 4491–4512.
Schneider von Deimling, J., Rehder, G., Greinert, J., McGinnnis, D., Boetius, A., and Linke, P. (**2011**). "Quantification of seep-related methane gas emissions at Tommeliten, North Sea," Cont. Shelf Res. **31**(7), 867–878.
Transportation Research Board and National Research Council (**2003**). "Natural seepage of crude oil into the marine environment," in *Oil in the Sea III: Inputs, Fates, and Effects* (The National Academies Press., Washington, DC), pp. 191–192.
U.S. Energy Information Administration (**2016**). "Offshore oil production in deepwater and ultra-deepwater is increasing," available at https://www.eia.gov/todayinenergy/detail.php?id=28552 (Last viewed June 1, 2018).
U.S. EPA (**2007**). *Test Methods for Evaluating Solid Waste, Physical/Chemical Methods*, Pub. No. SW84, Third Edit., Updates I–IV (United States Environmental Protection Agency, Washington, D.C.).
U.S. Library of Congress (**2011**). *On Scene Coordinator Report: Deepwater Horizon Oil Spill* (United States Dept. of Homeland Security, United States Coast Guard, Washington, D.C.).
Vazquez, D., and Mansoori, G. A. (**2000**). "Identification and measurement of petroleum precipitates," J. Pet. Sci. Eng. **26**(1–4), 49–55.
Weber, T. C., De Robertis, A., Greenaway, S. F., Smith, S., Mayer, L., and Rice, G. (**2012**). "Estimating oil concentration and flow rate with calibrated vessel-mounted acoustic echo sounders.," Proc. Natl. Acad. Sci. U.S.A. **109**(50), 20240–20245.
Weber, T. C., Mayer, L., Jerram, K., Beaudoin, J., Rzhanov, Y., and Lovalvo, D. (**2014**). "Acoustic estimates of methane gas flux from the seabed in a 6000 km^2 region in the Northern Gulf of Mexico," Geochem., Geophys., Geosyst. **15**(5), 1911–1925, https://doi.org/10.1002/2014GC005271
Wilkinson, J. P., Boyd, T., Hagen, B., Maksym, T., Pegau, S., Roman, C., Singh, H., and Zabilansky, L. (**2015**). "Detection and quantification of oil under sea ice: The view from below," Cold Reg. Sci. Technol. **109**, 9–17.
Wunderlich, B. (**1990**). *Thermal Analysis* (Academic, Boston).